Accurate *ab initio* potential energy curve of O_2. II. Core-valence correlations, relativistic contributions, and vibration-rotation spectrum

Laimutis Bytautas,[1,a)] Nikita Matsunaga,[2,b)] and Klaus Ruedenberg[1,c)]
[1]*Department of Chemistry and Ames Laboratory (USDOE), Iowa State University, Ames, Iowa 50011, USA*
[2]*Department of Chemistry and Biochemistry, Long Island University, Brooklyn, New York 11201, USA*

(Received 10 November 2009; accepted 4 January 2010; published online 19 February 2010)

In the first paper of this series, a very accurate *ab initio* potential energy curve of the $^3\Sigma_g^-$ ground state of O_2 has been determined in the approximation that all valence shell electron correlations were calculated at the complete basis set limit. In the present study, the corrections arising from *core* electron correlations and relativity effects, *viz.*, spin-orbit coupling and scalar relativity, are determined and added to the potential energy curve. From the 24 points calculated on this curve, an analytical expression in terms of even-tempered Gaussian functions is determined and, from it, the vibrational and rotational energy levels are calculated by means of the discrete variable representation. We find 42 vibrational levels. Experimental data (from the Schumann–Runge band system) only yield the lowest 36 levels due to significant reduction in the transition intensities of higher levels. For the 35 term values G(v), the mean absolute deviation between theoretical and experimental data is 12.8 cm^{-1}. The dissociation energy with respect to the lowest vibrational energy is calculated within 25 cm^{-1} of the experimental value of 41 268.2 ± 3 cm^{-1}. The theoretical crossing between the $^3\Sigma_g^-$ state and the $^1\Sigma_g^+$ state is found to occur at 2.22 Å and the spin-orbit coupling in this region is analyzed. © *2010 American Institute of Physics*. [doi:10.1063/1.3298376]

I. INTRODUCTION

Oxygen is of great significance in biological, combustion, and atmospheric chemistry as well as in many other processes. It is reckoned[1–4] that the appearance of O_2 in the environment, around 2.2×10^9 years ago, had a revolutionizing effect on biochemical networks and the evolution of complex life. The ground state of O_2 is a triplet. Since the majority of the reactions with organic molecules are with singlets, they are spin forbidden implying that they are slow at ambient conditions, a circumstance that represents a problem for living organisms wanting to employ O_2 in their metabolism. It appears that nature made use of transition metals to carry, activate, and reduce O_2, as for instance in the binding of O_2 to Fe in hemoglobin.[5] It is also well known[6] that the singlet excited state $^1\Delta_g$ exhibits a high reactivity and contributes to the degradation of biological cells. Oxygen furthermore plays a key role in the chemistry of the Earth's atmosphere. The splitting of the oxygen bond in O_2 by ultraviolet solar radiation is the primary step in the formation of O_3, and hence essential for the ozone layer.[7] Studies focusing on the UV photodissociation of O_2 therefore received much attention in recent years.[8–11] The O_2 molecule manifestly plays a manifold role in the maintenance of life on earth.

A major tool for understanding molecular electronic structures are spectroscopic measurements of vibrational levels that yield information about potential energy surfaces.[12–15] While in certain cases, e.g., the Be_2 molecule,[16] spectroscopic experiments yielded *all* vibrational levels of the molecule, this is unfortunately not always so. One of the difficult cases in this regard is the oxygen molecule and, although continuous improvements have been made over the years,[17–19] its complete ground state spectrum is not yet known experimentally. The existing spectroscopic data for the vibrational and rotational levels in the ground electronic state ($^3\Sigma_g^-$) come almost entirely from observations on the very strong ($X\ ^3\Sigma_g^- - B\ ^3\Sigma_u^-$) Schumann–Runge band[20,21] and the intensities of its high terms are greatly weakened due to a predissociation of the B-state.[18,19] This makes the determination of the complete vibrational spectrum of the ($^3\Sigma_g^-$) state a challenging task[22–27] and its higher vibrational levels were only rather recently reported. The vibrational levels up to v = 28 were determined by Creek and Nicholls,[24] up to v = 31 by Jongma *et al.*,[27] and up to v = 35 by Yang and Wodtke.[26] In spite of this considerable increase in the experimental information, the highest level v = 35 lies still about 1400 cm^{-1} below the separated atom limit while the spacing between levels 34 and 35 is 562 cm^{-1}, which suggests the existence of additional levels. The experimental determination of $D_0(X)$ has been the focus of numerous studies[28–32] with numerical values ranging from 41 256.6 (Ref. 30) to 41 269.6 cm^{-1}.[31] The most recent experimental dissociation energy of $D_0(X) = 41\ 268.2 \pm 3\ cm^{-1}$ was reported by Ruscic *et al.* in 2004.[28]

Ab initio methods can generate the full potential energy curve (PEC) from which the experimentally missing levels

[a)]Electronic mail: bytautas@scl.ameslab.gov.
[b)]Electronic mail: nikita.matsunaga@liu.edu.
[c)]Electronic mail: ruedenberg@iastate.edu.

TABLE I. Contributions to the ground state PEC of O_2. Energies are in millihartree.

R (Å)	Valence[a]	Scalar rel.	Core-corr.	SO	Total PEC
0.900 00	112.263	−0.010	−4.131	0.731	108.852
0.950 00	−7.699	0.172	−3.294	0.731	−10.090
1.000 00	−87.790	0.282	−2.572	0.731	−89.349
1.050 00	−139.427	0.339	−1.949	0.731	−140.306
1.100 00	−170.314	0.358	−1.411	0.731	−170.637
1.125 00	−179.879	0.356	−1.171	0.731	−179.963
1.150 00	−186.344	0.350	−0.950	0.730	−186.214
1.175 00	−190.182	0.339	−0.745	0.730	−189.858
1.207 52	**−192.012**	**0.320**	**−0.503**	**0.730**	**−191.464**
1.250 00	−190.047	0.290	−0.224	0.730	−189.251
1.300 00	−183.345	0.251	0.055	0.730	−182.309
1.350 00	−173.258	0.211	0.288	0.729	−172.030
1.400 00	−161.007	0.174	0.479	0.729	−159.625
1.500 00	−133.467	0.109	0.757	0.729	−131.872
1.600 00	−105.442	0.059	0.923	0.728	−103.732
1.700 00	−79.313	0.024	0.992	0.728	−77.568
1.800 00	−56.596	0.000	0.974	0.726	−54.897
2.000 00	−23.621	−0.020	0.711	0.718	−22.212
2.200 00	−8.520	−0.016	0.359	0.697	−7.480
2.400 00	−3.658	−0.009	0.164	0.650	−2.853
2.600 00	−2.064	−0.004	0.061	0.549	−1.458
2.800 00	−1.359	−0.002	0.032	0.462	−0.867
3.000 00	−1.010	−0.001	0.019	0.276	−0.716
6.000 00	0.0	0.0	0.0	0.0	0.000

[a]From the last column of Table IV in Ref. 33.

can be obtained by solving the rovibrational Schrödinger equation. The main problem here is the achievement of the accuracy required to produce a credible vibration spectrum, which can of course be assessed by how well the 36 known levels are recovered. In the preceding paper of the present series,[33] we calculated the O_2 ground-state PEC taking into account electron correlation in the valence shell by near-full configuration interaction, complemented by complete basis set (CBS) extrapolation. In the present study we calculate the correlation energy associated with the core electrons, the contributions from spin-orbit (SO) coupling, and scalar relativistic effects, and add these corrections to obtain points on the final PEC. An even tempered analytical fit to these points is then used in the solution of the rovibrational Schrödinger equation. We obtain 42 vibrational levels for the ground state PEC, i.e., six levels beyond the so far measured spectrum. The mean absolute deviation (MAD) from the experimental data up to $v=35$ is 12.8 cm^{-1}. The excellent agreement of theory with experiment found for this 16 electron molecule as well as for the earlier reported 18-electron F_2 molecule[34–37] suggests that first-principles electronic calculations will become useful in elucidating rovibrational spectra for first-row diatomic molecules.

There exist prior *ab initio* studies[38,39] on the rovibrational spectra of the $^3\Sigma_g^-$ ground state of O_2. The earliest such calculation appears to be the one reported by Guberman[38] in 1977, which was based on CI wave functions including only double-zeta basis sets, only single excitations into nonvalence-space orbitals, and no further refinements. The binding energy was too low by about 8 mhartree and the spectrum contained only 32 levels. It yielded however surprisingly good values for the lower levels. Recently, Varandas[39] calculated a PEC using the MRCISD+Q method and extrapolated it to the CBS limit. From this curve he determined 22 vibrational levels with a root-mean-square-deviation of about 40 cm^{-1} from the experimental spectrum. Neither Guberman[38] nor Varandas[39] included however the effects associated with core correlation, SO coupling, and scalar relativity. It should also be noted that *ab initio* studies have provided useful information for excited states,[40–42] in which there is a considerable interest.

In the following, we shall first discuss the calculation of the additional corrections due to core correlation, to SO coupling, and to scalar relativistic effects. Next, the analytic fit of the total PEC is determined. Then the rotation-vibration spectrum is obtained. Finally, the theoretical results are compared with the available experimental data.

II. *AB INITIO* POTENTIAL ENERGY CURVE

Table I collects the *corrections to the PEC* that were determined in the first paper of this series.[33] The first column lists the 24 internuclear distances considered. The second column lists the values obtained for the PEC in the first paper,[33] where the CBS limits of the valence shell correlations were determined by near-full CI-correlation energy extrapolation by intrinsic scaling (CEEIS) calculations. Columns 3–5 list the corrections that will be determined in the flowing three subsections. The last column contains the corrected PEC.

A. Correlation energy contributions involving core electrons

In the oxygen molecule the electron correlations involving core orbitals lower the total energy by about 120–130 mhartree, i.e., ~25% of the valence correlation energy at the equilibrium geometry, which is similar to what was found in F_2.[35] Along the dissociation path, this core contribution changes however by rather small amounts compared to the valence correlation changes. The correlation energy *changes* along the reaction paths contributed by core involvement can therefore be calculated by wave functions with a lower correlation recovery than that achieved for the correlations in the valence space in the preceding paper.[33] The method must be based though on a multiconfigurational reference function that is capable of properly representing the dissociation without deterioration at stretched geometries. As in the case of F_2, we chose the second-order multireference configuration interaction approach with the Davidson correction (MRCISD+Q), which has proven to be sufficiently accurate in the present context.[39,43] Moreover, while Dunning's valence correlation-consistent cc-pVXZ basis sets[44] were appropriate for the recovery of the valence correlation energy, the more elaborate cc-pCVXZ core-valence basis sets of Dunning and co-workers[45] must be used to calculate core correlation effects. The energies were calculated with the cc-pCVTZ and cc-pCVQZ basis sets and then extrapolated to the CBS limits in standard fashion.[46,47] In this manner, we calculated the energies along the dissociation path when *all* electrons are correlated as well as the energies when only the valence electrons are correlated. The difference between these two energies yielded the correlation contributions that are generated by the core electrons. All calculations were performed with the GAMESS suite of quantum chemical[48,49] programs.

The first step in the application of the MRCI method is the determination of the full optimized reaction space (FORS) molecular orbitals,

$$1\sigma_g, 1\sigma_u, 2\sigma_g, 2\sigma_u, 3\sigma_g, 3\sigma_u, 1\pi x_u, 1\pi y_u, 1\pi x_g, 1\pi y_g, \quad (1)$$

for the construction of the reference functions along the dissociation path. Here and in the following, we use the nomenclature of Ref. 50: CASSCF (complete active space) as a generic term, FORS=CASSCF generated by a full space of valence orbitals, reduced full orbital reaction (RFORS) space, if certain subspaces of FORS are considered.

When the FORS[12/8] function is MCSCF optimized, the $2\sigma_g$, $2\sigma_u$ orbitals turn out to be doubly occupied for large R and, as a result, they mix with the $1\sigma_g$, $1\sigma_u$ orbitals. Such mixing interferes with the correct subsequent construction of excited configurations for the *valence-only* MRCI calculations and, hence, leads to spurious correlation energy fluctuations. This complication was avoided by first optimizing all orbitals using a RFORS [8/6] wave function whose active orbitals were only the six orbitals, $3\sigma_g$, $3\sigma_u$, $1\pi x_u$, $1\pi y_u$, $1\pi x_g$, and $1\pi y_g$, keeping the orbitals $1\sigma_g$, $1\sigma_u$, $2\sigma_g$, and $2\sigma_u$ inactive, and then diagonalizing the Fock matrix of the *inactive* orbitals. The resulting MOs of the list (1), expressed in terms of the cc-pCVXZ basis set (X=3,4), were then used for both the valence-only as well as the all-electron MRCISD+Q calculations.

TABLE II. Core-correlation contributions to the ground state PEC of O_2 calculated using the MRCISD+Q method. Energies are in millihartree.

R (Å)	cc-pCVTZ	cc-pCVQZ	CBS-limit	PEC[a]
0.900 00	−108.882 430	−120.023 120	−128.152 81	−4.131
0.950 00	−108.261 690	−119.277 229	−127.315 60	−3.294
1.000 00	−107.720 893	−118.631 780	−126.593 78	−2.572
1.050 00	−107.249 957	−118.072 582	−125.970 17	−1.949
1.100 00	−106.841 032	−117.589 194	−125.432 45	−1.411
1.125 00	−106.657 802	−117.373 311	−125.192 74	−1.171
1.150 00	−106.487 768	−117.173 399	−124.971 02	−0.950
1.175 00	−106.330 253	−116.988 610	−124.766 33	−0.745
1.207 52	**−106.143 102**	**−116.769 540**	**−124.523 97**	**−0.503**
1.250 00	−105.926 766	−116.517 000	−124.245 01	−0.224
1.300 00	−105.709 436	−116.263 976	−123.965 94	0.055
1.350 00	−105.528 293	−116.053 393	−123.733 87	0.288
1.400 00	−105.379 258	−115.880 065	−123.542 82	0.479
1.500 00	−105.163 488	−115.627 792	−123.263 91	0.757
1.600 00	−105.039 210	−115.479 627	−123.098 31	0.923
1.700 00	−104.991 545	−115.419 416	−123.028 94	0.992
1.800 00	−105.010 936	−115.438 452	−123.047 72	0.974
2.000 00	−105.203 444	−115.671 553	−123.310 44	0.711
2.200 00	−105.431 057	−115.970 826	−123.662 01	0.359
2.400 00	−105.545 993	−116.132 369	−123.857 56	0.164
2.600 00	−105.590 243	⋯	⋯	0.061[b]
2.800 00	−105.608 571	⋯	⋯	0.032[b]
3.000 00	−105.617 384	⋯	⋯	0.019[b]
6.000 00	−105.630 922	−116.262 913	−124.021 39	0.000

[a]Contribution to the PEC at the CBS limit: PEC=E(CBS,R) −E(CBS,6 Å).
[b]Estimated from cc-pCVTZ calculations.

To be consistent with the valence-correlation-only calculations of the preceding paper,[33] the *reference* functions for the valence-only MRCISD+Q calculations were the CI wave functions in the full FORS[12/8] configuration space generated by the 12 valence electrons using the last 8 orbitals of list (1) as active orbitals, while keeping both 1σ orbitals doubly occupied. Single and double excitations were then generated by moving electrons from the eight valence orbitals into virtual orbitals. Analogously, the reference functions for the *all-electron* MRCISD+Q calculations were the CI wave functions in the full configuration space generated by all 16 electrons using all 10 MOs of list (1) as active orbitals. Single and double excitations were then generated by moving electrons from all ten reference orbitals into virtual orbitals.

The results are listed in the fourth column of Table II. The first column gives the internuclear distances along the reaction path. Columns 2–4 list, respectively, the corresponding energy contribution due to core electrons for the cc-pCVTZ and the cc-pCVQZ basis sets and the CBS limit. The last column lists the core-correlation contribution *to the PEC*, calculated as E(CBS,R)−E(CBS,6 Å). Since the nuclear charge of oxygen is less than that of fluorine, the core electrons in O_2 are not quite as tightly bound as in F_2 and the core-correlation effect is stronger in O_2 than in F_2. The comparison of the data in Table II with those in Table IV

TABLE III. Scalar relativistic energy (mass-velocity+Darwin) contributions for the ground state PEC of O_2, calculated using RFORS [8/6] wave function and cc-pCVQZ basis sets.

R (Å)	RFORS[8/6] (hartree)	RFORS+DK3 (hartree)	ΔDK [a] (mhartree)	PEC[b] (mhartree)
0.900 00	−149.457 217	−149.561 699	−104.482	−0.010
0.950 00	−149.577 284	−149.681 584	−104.300	0.172
1.000 00	−149.657 841	−149.762 031	−104.190	0.282
1.050 00	−149.709 731	−149.813 864	−104.133	0.339
1.100 00	−149.740 945	−149.845 060	−104.115	0.358
1.125 00	−149.750 706	−149.854 822	−104.116	0.356
1.150 00	−149.757 373	−149.861 496	−104.123	0.350
1.175 00	−149.761 445	−149.865 579	−104.134	0.339
1.207 52	**−149.763 549**	**−149.867 702**	**−104.153**	**0.320**
1.250 00	−149.762 041	−149.866 224	−104.183	0.290
1.300 00	−149.755 780	−149.860 002	−104.222	0.251
1.350 00	−149.746 261	−149.850 523	−104.261	0.211
1.400 00	−149.734 726	−149.839 025	−104.299	0.174
1.500 00	−149.709 021	−149.813 385	−104.364	0.109
1.600 00	−149.683 507	−149.787 921	−104.413	0.059
1.700 00	−149.660 923	−149.765 371	−104.449	0.024
1.800 00	−149.642 830	−149.747 302	−104.473	0.000
2.000 00	−149.622 252	−149.726 745	−104.493	−0.020
2.200 00	−149.617 091	−149.721 580	−104.489	−0.016
2.400 00	−149.616 872	−149.721 353	−104.481	−0.009
2.600 00	−149.617 265	−149.721 742	−104.477	−0.004
2.800 00	−149.617 539	−149.722 013	−104.474	−0.002
3.000 00	−149.617 676	−149.722 149	−104.473	−0.001
6.000 00	−149.617 777	−149.722 250	−104.472	0.0

[a]Scalar relativistic correction: ΔDK=(RFORS+DK3)−(RFORS[8/6])
[b]Contribution to the PEC=ΔDK(R)−ΔDK(6 Å).

TABLE IV. Symmetries, spin states, and dissociative ionicities of RFORS[8/6] space of O_2. Without brackets: number of states. Within brackets: number of orthogonal CSFs.

Irrp	Ionicity	S=0 (dim)[a]	S=1 (dim)[a]	S=2(dim)[a]	Total (dim)[a]
Σ^+	0/0	8 (8)	4 (12)	2 (10)	14 (30)
	+/−	3 (3)	3 (9)		6 (12)
	2+/2−	2 (2)			2 (2)
	Total	18 (18)	10 (30)	2 (10)	30 (58)
Σ^-	0/0	3 (3)	7 (21)	1 (5)	11 (29)
	+/−	3 (3)	4 (12)	1 (5)	8 (20)
	2+/2−		1 (3)		1 (3)
	Total	9 (9)	17 (51)	3 (15)	29 (75)
Π	0/0	8 (16)	10 (60)	2 (20)	20 (96)
	+/−	5 (10)	6 (36)	1 (10)	12 (56)
	2+/2−	1 (2)	1 (6)		2 (8)
	Total	20 (40)	24 (144)	4 (40)	48 (224)
Δ	0/0	6 (12)	5 (30)	1 (10)	12 (52)
	+/−	3 (6)	3 (18)		6 (24)
	2+/2−	1 (2)			1 (2)
	Total	14 (28)	11 (66)	1 (10)	26 (104)
Φ	0/0	2 (4)	2 (12)		4 (16)
	+/−	1 (2)	1 (6)		2 (8)
	Total	4 (8)	4 (24)		8 (32)
Γ	0/0	1 (2)			1 (2)
	Total	1 (2)			1 (2)
TOTALS					
	0/0	28 (45)	28 (135)	6 (45)	62 (225)
	+/−	15 (24)	17 (81)	2 (15)	34 (120)
	−/+	15 (24)	17 (81)	2 (15)	34 (120)
	2+/2−	4 (6)	2 (9)		6 (15)
	2−/2+	4 (6)	2 (9)		6 (15)
ALL		66 (105)	66 (315)	10 (75)	142 (495)
$M_s = 0$		(105)	(105)	(15)	(225)
$M_s = \pm 1$			(105)	(15)	(120)
$M_s = \pm 2$				(15)	(150)

[a] (dim) = dimension counting +/− and −/+, as well as M_s = 0,1,2, or as specified.

of Ref. 35 shows that this holds along the entire dissociation curve. The values of the core correlation contributions to the PEC obtained by these MRCISD+Q calculations are also entered in the fourth column of Table I.

B. Scalar relativistic energy contributions

As in our study of F_2,[35] we used the one-electron Douglas–Kroll (DK) approach,[51–55] including the transformation to third order (DK3), to calculate the scalar relativistic mass-velocity-plus-Darwin energy corrections.[55–58] We used the code due to Nakajima and Hirao[59,60] and to Fedorov *et al.*,[61] which is implemented in GAMESS.[48,49]

As discussed in Ref. 35, the scalar relativistic corrections can be adequately calculated from RFORS[8/6]-MCSCF wave functions in terms of cc-pCVQZ basis sets. The results are reported in Table III. The first column gives the internuclear distances, and the second and third columns report the total energies for the RFORS[8/6] wave functions calculated without and with the DK3 term, respectively. Column 4 lists the energy contribution due to scalar relativity calculated by subtracting column 2 from column 3. Finally, column 5 lists the scalar relativity contribution to the dissociation curve calculated as E(R)−E(6 Å). It is apparent that, while the scalar relativistic corrections have magnitudes of about 100 mhartree, they change by less than a millihartree along the dissociation path. These changes are nonetheless non-negligible in the calculation of the vibrational levels. The values of column 5 of Table III are also entered in the third column of Table I.

C. Spin-orbit coupling contributions

Several methodologies exist to calculate SO coupling contributions to molecular energies.[54,62–64] Most rigorous are four-component methods based on the Dirac equation. The challenges of this approach are avoided by two-component methods that are derived by separating the large from the small components. Complementation by the interelectronic couplings leads to the Breit–Pauli operator,[62,65,66] which is the basis of the present work. The calculations were performed using the program by Fedorov *et al.*,[54,62] which is implemented in GAMESS,[48,49] including the full one- and two-electron terms. All calculations were performed with cc-pVQZ basis sets,[44] unless specifically stated otherwise.

The SO contributions to the ground state result from the diagonalization of the SO interaction matrix over a number of states in addition to the ground state. The choice of these states and of the orbitals from which they are constructed is consequential. We therefore discuss these first.

1. Reduced full valence configuration space

Since spin-obit coupling is a small correction for the lighter atoms, it can be determined at a lower level of corre-

lation and then added to the highly correlated wave function obtained in the first paper in this series.[33] Some of our SO interaction calculations are performed in the *full* valence space of O_2, which is spanned by 7280 orthogonal configurational state functions (CSFs) (superposition of determinants), of which 784 have $M_S=0$. For most of the dissociation curve, we are using the "reduced full valence space" of the molecule. The *reduced* full valence space[67–69] is obtained by having the six valence orbitals that are formed from the atomic 2p-orbitals occupied in all possible ways by eight electrons, while keeping the 2s orbitals on both oxygen atoms doubly occupied (RFORS[8/6]).

This configuration space consists of 142 states that can be characterized[10,70,71] by their symmetries $(\Sigma^+,\Sigma^-,\Pi,\Delta,\Phi,\Gamma)$, by their spin multiplicities $(S=0,1,2)$ and by the ionic characters of the dissociation products. The breakdown of this configuration space according to these criteria is documented in Table IV, in which the numbers without brackets denote the number of states in each category whereas the numbers in brackets indicate the corresponding number of actual orthogonal CSFs, if one counts space and spin degeneracies. By virtue of these degeneracies, the total space is seen to be spanned by 495 determinants, of which 225 have $M_S=0$. These 225 determinants span the space in which the CI diagonalizations take place for the various MCSCF calculations to be discussed below.

Upon dissociation the 142 molecular states mentioned above become combinations of the states of the $2s^22p^n$ configurations in the separate atoms,[10,70,71] namely, $(^3P,^1D,^1S)$ in O, $(^4S,^2D,^2P)$ in O^+, (^2P) in O^-, $(^3P,^1D,^1S)$ in O^{2+}, and (^1S) in O^{2-}. How many of the various molecular states dissociate into anyone of the various possible limiting combinations of atomic states is documented in Table V. The total configuration space dimensions, counting all degeneracies, are only given for the total of every limiting state combination. They are in the last two rows and indicated by brackets. It is seen that 62 states of the reduced full valence space dissociate into two neutral atoms. Counting the space and spin degeneracies, they span a CSF space of dimension 225 (not to be confused with the same numerical value at the end of the previous paragraph) and 99 of these have $M_S=0$.

To provide at least some quantitative perspective, Fig. 1 exhibits plots of these 62 states, obtained by an MCSCF calculation in the 225 dimensional CI space for $M_S=0$, which was identified at the end of the paragraph *before* the preceding paragraph, and state-averaged over the 99 CSFs mentioned at the end of the preceding paragraph. They are seen to dissociate indeed into the combination of neutral atom states indicated in columns 2–7 of Table V.

2. States originating from the ^3P-^3P limit of the separated atom ground states

According to Table V and Fig. 1 there are 18 states (out of the 62) that dissociate into the ^3P-^3P limit of the separated atom ground states. Taking into account all space and spin degeneracies, these 18 states span an 81 dimensional CSF space, which contains 27 determinants with $M_S=0$. Among these 18 states, there are six bound states with the respective symmetries $^3\Sigma_g^-$, $^1\Delta_g$, $^1\Sigma_g^+$, $^1\Sigma_u^-$, $^3\Delta_u$, and $^3\Sigma_u^+$, shown at the lower left of Fig. 1, between which radiative transitions are dipole forbidden[18,72] The ungerade states have recently been studied in detail in the long-range region by van Vroonhoven and Groenenboom.[10,11]

Most important are the three low lying bonding states, $^3\Sigma_g^-$, $^1\Delta_g$, and $^1\Sigma_g^+$. We obtained very accurate PECs for the two excited states, $^1\Delta_g$ and $^1\Sigma_g^+$, by determining the CBS

TABLE V. Dissociation of RFORS[8/6] states of O_2 into combinations of states of the separated atoms.

O_2	O/O							O^+/O^- & O^-/O^+				O^{2+}/O^{2-} & O^{2-}/O^{2+}				O_2
	$^3P/^3P$	$^3P/^1D$	$^1D/^1D$	$^3P/^1S$	$^1D/^1S$	$^1S/^1S$	Tot	$^2P/^2P$	$^2P/^2D$	$^2P/^4S$	Tot	$^1S/^3P$	$^1S/^1D$	$^1S/^1S$	Tot	TOT
$^1\Sigma^+$	2		3		2	1	8	4	2		6		2	2	4	18
$^3\Sigma^+$	2	2					4	4	2		6					10
$^5\Sigma^+$	2						2									2
$^1\Sigma^-$	1		2				2	2	4		6					9
$^3\Sigma^-$	1	4		2			7	2	4	2	8	2			2	17
$^5\Sigma^-$	1						1			2	2					3
$^1\Pi$	2		4		2		8	4	6		10		2		2	20
$^3\Pi$	2	6		2			10	4	6	2	12	2			2	24
$^5\Pi$	2						2			2	2					4
$^1\Delta$	1		3		2		6	2	4		6		2		2	14
$^3\Delta$	1	4					5	2	4		6					11
$^5\Delta$	1						1									1
$^1\Phi$			2				2		2		2					4
$^3\Phi$		2					2		2		2					4
$^1\Gamma$			1				1									1
TOT	18	18	15	4	6	1	62	24	36	8	68	4	6	2	12	142
D [a]	(81)	(90)	(25)	(18)	(10)	(1)	(225)	(72)	(120)	(48)	(240)	(18)	(10)	(2)	(30)	(495)
D_o [b]	(27)	(30)	(25)	(6)	(10)	(1)	(99)	(36)	(60)	(12)	(108)	(6)	(10)	(2)	(18)	(225)

[a] D = dimension including $M_s = 0,1,2$.

[b] D_o = dimension for $M_s = 0$.

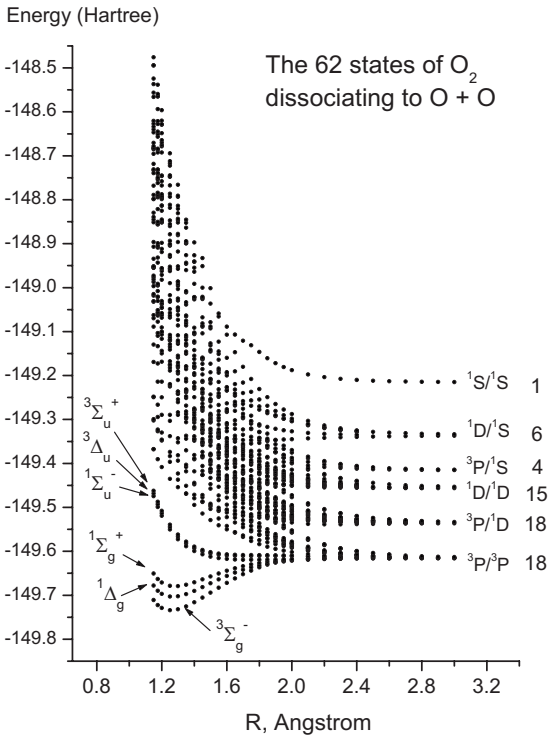

FIG. 1. The 62 states of the reduced full valence space of O_2 that dissociate into neutral atoms, obtained by state-averaged MCSCF calculation with a cc-pVQZ basis.

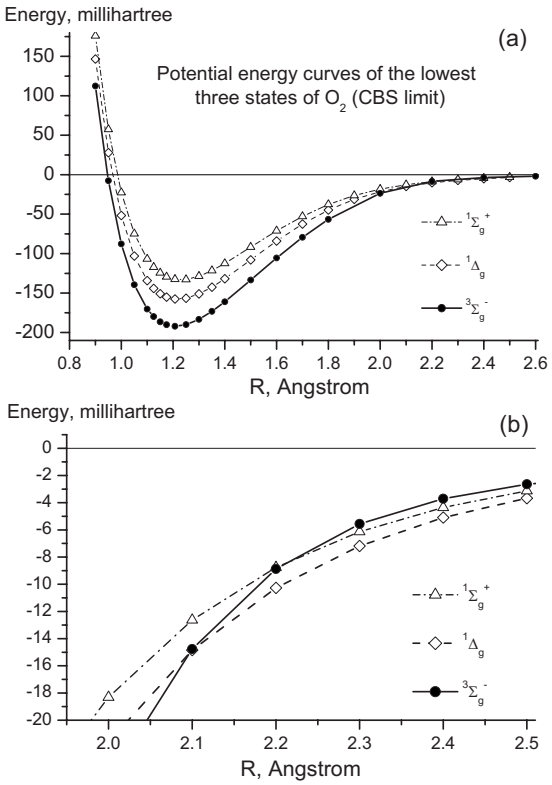

FIG. 2. The lowest three states of O_2: $^3\Sigma_g^-$, $^1\Delta_g$, and $^1\Sigma_g^+$. Upper panel (a): global plots. Lower panel (b): enlargement of the region where the states cross. Included is the valence electron correlation at the CBS limit. Near-full CI for $^3\Sigma_g^-$, MRCISD+Q for $^1\Delta_g$ and $^1\Sigma_g^+$.

limits of MRCISD+Q calculations with respect to the *full valence space of 12 electrons in 8 orbitals (FORS[12/8]).* The orbitals for these calculations were obtained from preliminary MCSCF calculations state-averaged over the four $M_S=0$ components of the states $^3\Sigma_g^-$, $^1\Delta_g$, and $^1\Sigma_g^+$. Figure 2 displays these $^1\Delta_g$ and $^1\Sigma_g^+$ PECs together with the near-full-CI-CEEIS curve of the $^3\Sigma_g^-$ ground state, which we obtained in the first paper of this series (see the last column of Table IV of Ref. 33). Figure 2(a) displays the global curves. Figure 2(b) exhibits an enlarged picture beyond 1.7 Å, which shows that, around 2 Å, the $^1\Delta_g$ and the $^1\Sigma_g^+$ states cross the $^3\Sigma_g^-$ ground state before all three come again together for the separated atoms. The corresponding quantitative data are listed in Tables SI and SII of the supplemental material.[73] The crossing region will be examined in more detail in Sec. II C 5.

Note that all three curves contain only valence correlations. Addition of the theoretical SO coupling energies, which will be discussed below (Sec. II C 4), to the curves of Fig. 2(a) yields the electronic binding energies 191.3, 156.8, and 132.0 mhartree for $^3\Sigma_g^-$, $^1\Delta_g$, and $^1\Sigma_g^+$ respectively, which compare well with the corresponding experimental values of 191.6, 155.5, and 131.4 mhartree.[18,28] Parenthetically, it may be noted that the $B^3\Sigma_u^-$ state, which gives rise to the Schumann–Runge transitions from the ground state $X^3\Sigma_g^-$, originates from the ^3P-^1D separate atoms limit.

3. Spin-orbit interaction space

As discussed in our study on F_2,[35] it is essential that the 2p-orbitals that are used for SO calculations are equivalent, especially at larger interatomic distances. This is accomplished by determining them through state-averaged MCSCF calculations over the 18 states that dissociate into the ^3P-^3P limit. Since these calculations are performed for $M_S=0$, this implies state averaging over all CI roots in the 27 dimensional determinant space specified in the first paragraph of Sec. II C 2. From these MCSCF orbitals, the *entire* configuration space of these same 18 states is then constructed, *including all possible space and spin degeneracies*, which consists of 81 determinants also mentioned at the beginning of Sec. II C 2. It is in this space that the Breit–Pauli operator is then diagonalized.

In the case of the oxygen atom, the SO interaction was calculated in the corresponding full 15 dimensional configuration space of four electrons in the three 2p-valence orbitals with the 2s-orbitals remaining doubly occupied (RFORS[4/3]). The orbitals were obtained from an MCSCF calculation state averaged over the three CSFs with $M_S=0$ of the ^3P state.

4. Spin-orbit coupling in the covalent range

Since either the spin or the orbital angular momentum or both vanish for the three *molecular* states, $^3\Sigma_g^-$, $^1\Delta_g$, and $^1\Sigma_g^+$, the SO coupling is very small at their equilibrium distances. The effect of this coupling on the respective dissociation energies is therefore essentially a decrease by twice the absolute value of the SO coupling of the ^3P state in the oxygen atom. The latter is given in Table VI, calculated at the same level of approximation as that used for the molecule, as described in the preceding section. The theoretical value of

TABLE VI. SO coupling in the oxygen atom.

State	$M_J=M_L+M_S$	RFORS[4/3][a] (hartree)	SO coupling (mhartree)	Level (cm^{-1})	Experiment[b] (cm^{-1})
$^3P_2$	0, ±1, ±2	−74.808 341	−0.366	0	0
$^3P_1$	0, ±1	−74.807 613	+0.362	159.8	158.3
$^3P_0$	0	−74.807 254	+0.721	238.4	227.0
$^1D_2$	0, ±1, ±2	−74.727 276	+0.003	17 791.9	15 867.9
$^1S_0$	0	−74.606 230	+0.004	44 358.9	33 792.6

[a]Energies from a CI calculations (using the cc-pVQZ basis) in the full reduced valence space generated by four electrons distributed in all possible ways over the three 2p-orbitals. The equivalent 2p-orbitals were obtained by a MCSCF calculation state averaged over the three spatial components of the ^3P state with $M_S=0$.
[b]See Ref. 74.

0.366 mhartree compares well with the experimental value of 0.344 mhartree.[27,74] It is apparent that, after SO coupling, the three molecular states considered will all go into the $^3P_2$-$^3P_2$ limit at infinite separation.

Since the z-component of the total angular momentum is a constant of the motion, only determinants with identical $M_J=M_L+M_S$ values are being mixed and the resulting states are characterized by the quantum number $\Omega=|M_J|$. The $^3\Sigma_g^-$ ground state, which is the focus of our interest, has a $\Omega=0$ component and two $\Omega=1$ components. Therefore, only the lowest SO-coupled states with these two Ω values are of interest in the present context. It is furthermore relevant that, of the two near-lying bound excited states, the $^1\Sigma_g^+$ state also has $\Omega=0$ and will therefore mix with the $\Omega=0$ component of the ground state under SO coupling, whereas the $^1\Delta_g$ state has only $\Omega=2$ components and therefore does not interact with the ground state.

The fifth column of Table I lists the SO contribution to the PEC for the $\Omega=1$ component of the $^3\Sigma_g^-$ ground state, which will be relevant for the vibration spectrum. The value at the equilibrium distance (0.730 mhartree) is almost exactly twice the absolute atomic value (0.366 mhartree) listed in row 1, column 4 of Table VI, which implies a molecular SO coupling of about 2 μhartree. The SO coupling for the $\Omega=0$ component of the $^3\Sigma_g^-$ ground state, on the other hand, is found to be −0.011 mhartree at the equilibrium distance, which is due to the interaction with the $^1\Sigma_g^+$ state mentioned above. Correspondingly, the SO coupling of the latter is +0.011 mh at the same distance. Thus, the $\Omega=0$ component of $^3\Sigma_g^-$ lies below its $\Omega=1$ component at all distances and is therefore strictly speaking the ground state.[75] The SO lowering of the $^1\Delta_g$ state is less than a microhartree. Manifestly, the energy changes due to these couplings are too small to visibly modify the curves of the three states on the scale of Fig. 2(a).

5. Spin-orbit coupling at larger distances

Figure 2(b) shows that the $^1\Delta_g$ and the $^1\Sigma_g^+$ states cross the $^3\Sigma_g^-$ ground state shortly beyond 2 Å. In light of the discussion in the second paragraph of the preceding section, it is apparent that the SO interaction between the $^1\Sigma_g^+$ state and the $^3\Sigma_g^-$ state will change the crossing between these two states into an avoided crossing, while it will not affect the crossing between the $^1\Delta_g$ state and the $^3\Sigma_g^-$ state. Since the avoided crossing between the two sigma states is surmised to be relevant for reactions resulting from collisions of two O_2 molecules[76–79] and is of interest to spectroscopists,[27] we examine it more carefully.

Figure 3 exhibits the Σ curves at the RFORS[8/6] level described in Sec. II C 3. The upper panel shows the crossing before SO coupling and the lower panel shows the avoided crossing after SO coupling. Figure 4 exhibits the analogous curves that are obtained if one uses a higher level of electron correlation recovery, namely, the multiconfiguration quasidegenerate second-order perturbation theory (MCQDPT2).[80,81] The quantitative energies for both approximations are listed in Table SIII of the supplemental material.[73] Quantitative information about the wave functions is given in Table SIV of the supplemental material.[73] These data confirm that 99% of

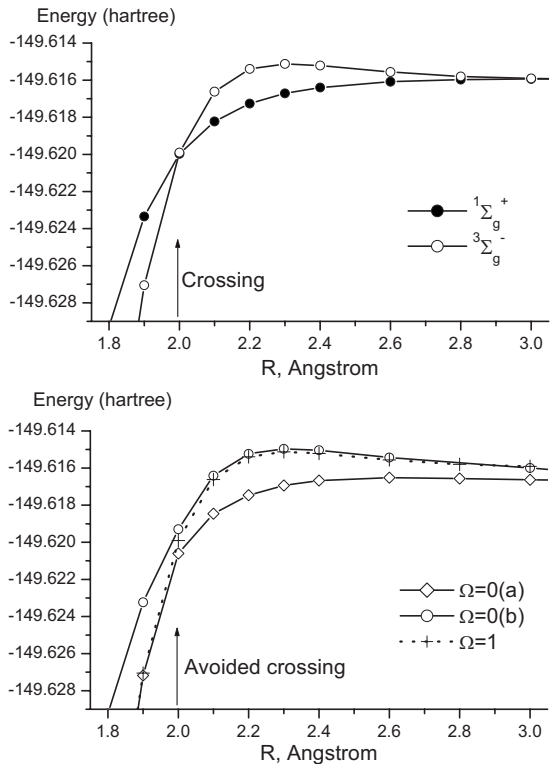

FIG. 3. SO interaction between the $^3\Sigma_g^-$ state and the $^1\Sigma_g^+$ state in the crossing region. Upper panel: $^3\Sigma_g^-$ and $^1\Sigma_g^+$ before SO coupling. Lower panel: the coupled states $\Omega=0$ (a), $\Omega=0$ (b), and $\Omega=1$ after SO coupling. The curves for $^1\Delta_g$ and $\Omega=2$ are omitted for the sake of clarity. SO interaction calculated in the space of all 18 states originating from the ^3P-^3P limit using a cc-pVQZ basis. The embedding CI space is that of eight electrons in the six 2p-generated orbitals RFORS[8/6].

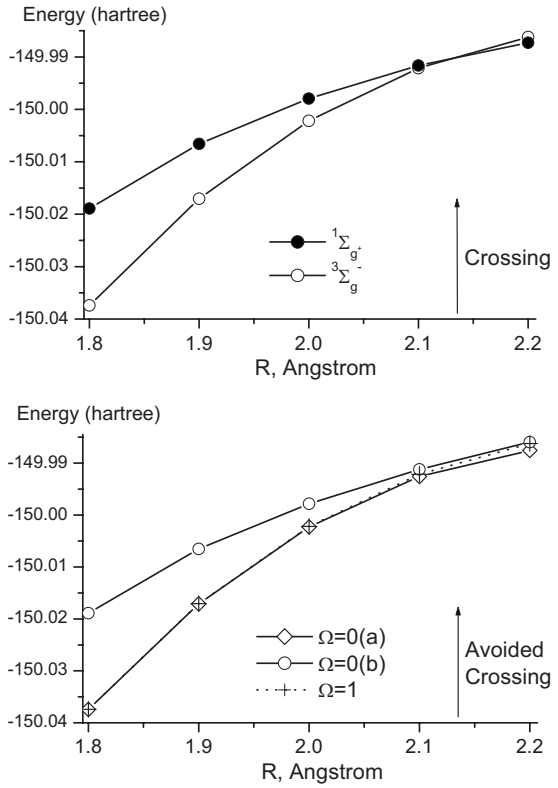

FIG. 4. SO interaction between the $^3\Sigma_g^-$ state and the $^1\Sigma_g^+$ state in the crossing region. Upper panel: $^3\Sigma_g^-$ and $^1\Sigma_g^+$ before SO coupling. Lower panel: the coupled states $\Omega=0$ (a), $\Omega=0$ (b), and $\Omega=1$ after SO coupling. The curves for $^1\Delta_g$ and $\Omega=2$ are omitted for the sake of clarity. SO interaction calculated in the space of all 18 states originating from the ^{3}P-^{3}P limit using a cc-pVQZ basis. The embedding CI space is that of 12 electrons in the full space of all 8 valence orbitals FORS[12/8].

the $\Omega=1$ state remains the $^3\Sigma_g^-$ state all the way as regards energy and wave function. On the other hand, the SO-coupled $\Omega=0$ states switch character from $^3\Sigma_g^-$ to $^1\Sigma_g^+$ and vice versa near the former intersection point.

The last section of Table SIII in the supplemental material[73] shows that, in this region, the energy lowering for the $\Omega=1$ state due to SO coupling is not changed by an increase in the dynamic correlation recovery. From its smallness, one can furthermore infer that the much larger splitting of the $\Omega=0$ states is essentially due to the interaction between $^3\Sigma_g^-$ and $^1\Sigma_g^+$. For a two-state interaction, the SO coupling matrix element between them would be related to the energies before and after coupling by

$$4\langle {}^1\Sigma_g^+|H_{SO}|{}^3\Sigma_g^-\rangle^2 = [E(\Omega=0b) - E(\Omega=0a)]^2 - [E({}^1\Sigma_g^+) - E({}^3\Sigma_g^-)]^2,$$

where $^3\Sigma_g^-$ and $^1\Sigma_g^+$ imply the $\Omega=0$ components. Using this formula with the energies in the first two sections of Table SIII in the supplemental material,[73] one finds the following absolute values for this "effective" interaction matrix element at the two levels of theory:

Absolute value of $\langle {}^1\Sigma_g^+(\Omega=0)|H_{SO}|{}^3\Sigma_g^-(\Omega=0)\rangle$ in mh.

R (Å)	1.8	1.9	2.0	2.1	2.2
RFORS[8/6]	0.69	0.68	0.65	0.63	0.61
(MCQDPT2)	0.72	0.69	0.66	0.63	0.59

The SO coupling for $\Omega=0$ is therefore also unaffected by the increase in correlation recovery. These values validate those obtained by Minaev and Yashchuk[69] using for H_{SO} a one-electron SO coupling operator with an effective nuclear charge.

However, Figs. 2(b), 3, and 4 show that the internuclear distance R_x where the two Σ curves intersect before SO coupling is sensitive to how much correlation is included. As a consequence, the calculations at the RFORS[8/6] and the (MCQDPT2) level give quite different values for the internuclear distance where the $\Omega=0$ and the $\Omega=1$ components of the $^3\Sigma_g^-$ state split apart (see Figs. 3 and 4).

The comparison of Figs. 2(b), 3, and 4 shows that the intersection distance R_x shifts to slightly longer distances with increasing correlation recovery:

Full CI in the reduced valence spaces of 8 electrons in six orbitals (RFORS[8/6]); cc-pVQZ basis	$R_x=1.98$ Å
MC quasidegenerate second-order perturbation theory based on the FORS[12/8] reference space; cc-pVQZ basis	$R_x=2.135$ Å
MRCISD+Q w/r to full space of 12 electrons in all eight valence orbitals (FORS[12/8]); CBS limit	$R_x=2.22$ Å.

Figure S1 of the supplementary material[73] shows that, for a double-zeta basis, the MRCISD+Q level theory yields a near identical R_x value as the MRCI-SDTQ level theory. Since it is reasonable to expect similar agreement for the CBS limit quoted above, it seems unlikely that R_x will move beyond 2.3 Å. The effect of the basis-set set size on R_x is documented in Fig. S2 of the supplementary material.[73] It shows that there is very little change in R_x from the cc-pVQZ basis to the CBS limit.

An earlier, slightly lower level theoretical study[82] predicted the value $R_x=2.17$ Å. Two deductions of the crossing distance R_x from experiment have been reported. Jongma *et al.*[27] deduced a value of $R_x=2.45\pm0.1$ Å by means of a perturbation extrapolation[83] based on a vibrational level degeneracy lying about 4500 cm^{-1} (ten levels) below the PEC value at R_x. More recently, Dayou *et al.*[79] obtained the value $R_x=2.154$ Å by deperturbation of an RKR curve based on the levels up to v=35.

Based on the RKR data, these authors[79] also reported that the $^3\Sigma_g^-$ state and $^1\Delta_g$ state cross at 2.09 Å. Our results in Table SIII (Ref. 73) yield the value of 2.10 Å for this crossing.

TABLE VII. Parameters of analytical even-tempered Gaussian expansions for the ground state PEC of O_2. Units: α in $Å^{-2}$. β=dimensionless. a_k in millihartree.

Parameters	CBS	CBS+SR	CBS+SR+SO	CBS+SR+SO+CV
α	0.776	0.777	0.785	0.785
β	1.305	1.305	1.305	1.307
a_0	−3035.985 960 7	−3036.174 514 8	−2472.440 309 5	−2388.564 169 0
a_1	21 761.455 801	21 765.115 885	18 628.304 847	18 086.977 116
a_2	−81 134.958 168	−81 269.488 310	−73 617.204 533	−71 760.197 585
a_3	169 079.247 09	169 677.149 30	158 601.837 75	154 738.091 75
a_4	−229 652.963 39	−229 652.963 39	−220 166.377 75	−215 074.856 46
a_5	224 424.374 91	226 100.115 22	219 028.327 03	214 799.545 67
a_6	−152 120.365 72	−153 566.587 53	−150 509.432 06	−148 395.428 50
a_7	73 193.717 160	73 878.865 565	73 440.404 500	73 310.781 453
RMSQD[a]	0.082	0.082	0.084	0.084

[a]Root-mean-square deviations from the respective theoretical data in millihartree.

D. Analytical representation of the potential energy curve

Since the experimental vibrational spectrum is derived from the electronic transition between two triplet states (the Schumann–Runge band system), it is readily seen that it is associated with the potential curve of the $\Omega=1$ component of the $^3\Sigma_g^-$ state after spin coupling. The latter should therefore be used for calculating the rotational-vibrational spectrum and comparing it with the experimental data.

The solution of the rovibrational Schrödinger equation is greatly facilitated by the availability of an analytical expression for the PEC because, then, molecular energies can be calculated at arbitrary points along the dissociation path.[84,85] To this end, we chose the expansion in terms of *even-tempered Gaussian functions*, which has proven enormously flexible and effective for the construction of radial parts of atomic basis orbitals for a quarter of a century.[86–88] We found in Ref. 36 that PECs can be expressed as even-tempered Gaussian expansions using only relatively few data points.

The most appropriate even tempered expansion for the calculated data of Table I was found to be

$$V(R) = \Sigma_k a_k \exp(-\alpha\beta^k R^2), \quad k = 0,1,2,\cdots 7. \tag{2}$$

The coefficients a_k were obtained by linear regression and the exponent parameters α and β by nonlinear minimization. In addition to fitting the 24 *ab initio* energies, the potential was forced to vanish at 1000 Å. We note that the long range $(1/R^n)$ dependence occurs for V(R) values that are too small to matter in the present context.

Table VII lists the parameter values in Eq. (2) for five fits, which represent the following approximations to the PEC:

(i) **CBS**=PEC obtained as the CBS limit of the valence-shell-only full CI correlation calculation, i.e., energies in column 2 of Table I.

(ii) **CBS+SR**=PEC containing, in addition to CBS, also the scalar relativity contributions, listed in column 3 of Table I.

(iii) **CBS+SR+SO**=PEC containing, in addition to **CBS+SR**, also the SO coupling contributions, listed in column 5 of Table I.

(iv) **CBS+SR+SO+CV**=PEC containing, in addition to **CBS+SR+SO** also the core-electron correlation contributions, listed in column 4 in Table I.

Thus, the **CBS+SR+SO+CV** potential represents the total PEC of the O_2 ground state listed in the last column of Table I.

In Fig. 5, we graphically compare this total analytical potential with the *ab initio* values from the last column of Table I and with the values that were derived by the RKR method[13] from the experimental levels by Krupenie.[17] The agreement between all three sets of data is manifestly very good. A more stringent test for the theoretical potential will be presented by comparing the calculated rotational-vibrational energy levels with the experimental levels,[24–27] to which we now turn.

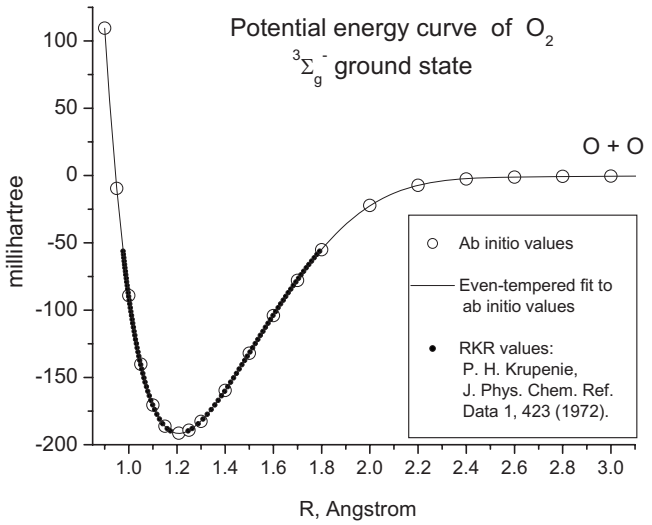

FIG. 5. The $^3\Sigma_g^-$ ($\Omega=1$) ground state PEC of O_2. Solid line: analytic even tempered fit to the *ab initio* energies indicated by empty circles. Solid dots: RKR values deduced from the experimental data in Ref. 17.

III. ROTATION-VIBRATION SPECTRUM

A. Solution of eigenvalue equation

The calculation of the rotational and vibrational energy levels $E_{v,J}$, where v and J are the vibrational and rotational quantum numbers, respectively, requires the solution of the nuclear Schrödinger equation,[89]

$$-(\hbar^2/2\mu)\partial^2 f(R)/\partial R^2 + [(\hbar^2/2\mu)J(J+1)/R^2 + V(R)]f(R) = E_{v,J}f(R), \quad (3)$$

where R is the internuclear distance, V(R) is one of the potential energy functions constructed in Sec. II D, and

$$f(R) = R \times \psi(R), \quad (4)$$

with $\psi(R)$ being the radial part of the wave function after factoring off the spherical harmonics containing the angular coordinates. According to the NIST database,[90] the value of the reduced mass μ of the two oxygen nuclei is 1/2 15.994 914 622 1 amu.

We used the discrete variable representation (DVR) of Light *et al.*[91,92] to solve Eq. (3), in the form it has been cast by Colbert and Miller.[93] These authors showed that the kinetic energy matrix in this representation can be chosen as

$$T_{ij} = [\hbar^2/(2\mu\Delta R^2)](-1)^{i-j}P_{ij}, \quad (5a)$$

where

$$P_{ij} = \pi^2/3 \quad \text{for} \quad i = j, \quad P_{ij} = 2/(i-j)^2 \quad \text{for} \quad i \neq j, \quad (5b)$$

and ΔR is the spacing of the grid. These equations follow, by differentiation, from the Lagrangian interpolation formula for equidistant arguments by extending the interpolated interval to plus or minus infinity while maintaining the fixed grid spacing. For a finite interpolation interval, they are valid, to a given accuracy, if the grid spacing ΔR is taken sufficiently small so that the number of grid points becomes sufficiently large. The potential energy operator V(R) on the other hand, being a local operator, is diagonal as in all grid-based representations. Unlike a basis expansion method, this approach requires no computation of integrals over basis functions. The eigenvalue problem for the matrix of the Hamiltonian of Eq. (3) was solved by the EISPACK subroutines.[94] The method is applicable for any value of J and in this study the $E_{v,J}$ values for J=0 to J=10 have been calculated.

The first grid point R_{in} and the last grid point R_{out} as well as the spacing ΔR of the even-spaced grid points in between were obtained by monitoring the vibrational energy levels as functions of these three parameters. The end points R_{in} and R_{out} were chosen such that the wave function of the highest energy level effectively converged to zero at these end points. The values R_{in}=0.5 bohr and R_{out}=14 bohr were found to be adequate. As the number of grid points between them was increased from 100 to 1000 in increments of 100, all calculated energy levels exhibited no further change when the number of grid points exceeded 300. We used 500 grid points in all our calculations, as in the previous study on F_2.[36]

TABLE VIII. Theoretical spectroscopic vibrational levels G_v, vibrational term values $G(v)=G_v-G_0$, and vibrational energy spacings $G_{v+1}-G_v$, calculated from the (CBS+SR+SO+CV) analytical potential of Table VII. Energies are in cm^{-1}.

v	G_v	G_v-G_0	$G_{v+1}-G_v$
0	791.64	0.00	⋯
1	2355.55	1563.91	1563.91
2	3894.05	3102.41	1538.50
3	5407.46	4615.82	1513.41
4	6896.11	6104.47	1488.65
5	8360.33	7568.69	1464.23
6	9800.47	9008.83	1440.14
7	11 216.85	10 425.21	1416.37
8	12 609.75	11 818.11	1392.91
9	13 979.46	13 187.82	1369.71
10	15 326.20	14 534.56	1346.74
11	16 650.15	15 858.51	1323.95
12	17 951.43	17 159.79	1301.28
13	19 230.12	18 438.48	1278.69
14	20 486.21	19 694.57	1256.09
15	21 719.63	20 927.98	1233.42
16	22 930.22	22 138.58	1210.60
17	24 117.78	23 326.14	1187.55
18	25 281.97	24 490.33	1164.19
19	26 422.40	25 630.76	1140.43
20	27 538.57	26 746.93	1116.17
21	28 629.87	27 838.22	1091.30
22	29 695.57	28 903.93	1065.70
23	30 734.84	29 943.20	1039.27
24	31 746.69	30 955.05	1011.85
25	32 729.97	31 938.33	983.28
26	33 683.36	32 891.72	953.39
27	34 605.32	33 813.68	921.96
28	35 494.06	34 702.42	888.73
29	36 347.45	35 555.81	853.39
30	37 162.99	36 371.35	815.54
31	37 937.66	37 146.02	774.67
32	38 667.75	37 876.11	730.10
33	39 348.62	38 556.98	680.87
34	39 974.23	39 182.59	625.61
35	40 536.37	39 744.72	562.14
36	41 023.12	40 231.48	486.76
37	41 415.58	40 623.94	392.46
38	41 682.68	40 891.04	267.10
39	41 822.31	41 030.67	139.63
40	41 921.19	41 129.55	98.88
41	41 996.26	41 204.62	75.07

Following spectroscopic conventions,[95] we express the rotation-vibration energy levels in the form

$$E_{v,J} = V_{eq} + G_v + F_v(J), \quad (6)$$

where V_{eq} is the minimum value of the potential V(R) in Eq. (3) at the equilibrium distance R_{eq}, and v and J are the vibrational and rotational quantum numbers, respectively. By definition $F_v(0)=0$ so that G_v is the pure vibrational term.

Since the rotational energy in Eq. (3) is very small compared to the vibrational energy, the rotational term $F_v(J)$ can be expanded as

TABLE IX. Comparison of the experimental term values $G(v)=G_v-G_0$ with the theoretical term values that are generated by a sequence of approximations to the full *ab initio* PEC. Energies are in cm^{-1}.

v	Experiment[a]	CBS[b]	CBS+SR [b]	CBS+SR+SO [b]	CBS+SR+SO+CV [b]
0	0	0	0	0	0
1	1 556.39	1.59	−0.58	−0.79	7.53
2	3 089.11	1.62	−2.70	−3.14	13.30
3	4 598.61	−0.04	−6.50	−7.16	17.21
4	6 084.69	−2.89	−11.46	−12.34	19.78
5	7 547.69	−6.96	−17.61	−18.68	21.00
6	8 988.14	−12.46	−25.16	−26.38	20.69
7	10 406.88	−19.92	−34.64	−35.96	18.33
8	11 801.67	−26.81	−43.51	−44.90	16.44
9	13 173.60	−33.97	−52.59	−54.00	14.22
10	14 523.24	−41.72	−62.23	−63.62	11.32
11	15 852.42	−51.73	−74.08	−75.41	6.09
12	17 156.56	−59.28	−83.42	−84.65	3.23
13	18 437.04	−65.68	−91.56	−92.67	1.44
14	19 695.20	−72.25	−99.82	−100.80	−0.63
15	20 930.90	−78.93	−108.14	−108.97	−2.92
16	22 143.10	−84.79	−115.60	−116.29	−4.52
17	23 331.50	−89.75	−122.12	−122.67	−5.36
18	24 497.11	−95.12	−129.00	−129.43	−6.78
19	25 638.53	−99.87	−135.23	−135.57	−7.77
20	26 755.46	−104.20	−141.00	−141.28	−8.53
21	27 847.50	−108.28	−146.48	−146.76	−9.28
22	28 914.05	−112.21	−151.79	−152.11	−10.12
23	29 954.28	−115.98	−156.92	−157.33	−11.08
24	30 967.58	−119.93	−162.21	−162.79	−12.53
25	31 952.62	−123.86	−167.47	−168.27	−14.29
26	32 908.37	−128.02	−172.95	−174.04	−16.65
27	33 833.11	−132.19	−178.46	−179.91	−19.43
28	34 723.69	−135.00	−182.60	−184.48	−21.27
29	35 581.93	−140.31	−189.28	−191.64	−26.12
30	36 399.63	−142.39	−192.76	−195.64	−28.28
31	37 175.38	−142.76	−194.58	−198.01	−29.36
32	37 897.00	−132.85	−186.19	−190.18	−20.89
33	38 552.00	−104.67	−159.62	−164.17	4.98
34	39 180.00	−103.66	−160.34	−165.40	2.59
35	39 760.00	−116.60	−175.18	−180.73	−15.28
MAD	⋯	80.24	112.39	113.89	12.84
ZPE	**787.20**[c]	**788.60**	**787.50**	**787.41**	**791.64**
D_e	**42 055.4 ± 3**[d]	**42 155.30**	**42 085.87**	**41 922.28**	**42 030.05**
R_e (Å)	**1.207 52**[e]	**1.210 19**	**1.210 43**	**1.210 41**	**1.207 81**

[a]See text regarding the sources.
[b]Listed are the deviations=(theory−experiment).
[c]See Ref. 24.
[d]See Ref. 28.
[e]See Ref. 95.

$$F_v(J) = B_v[J(J+1)] - D_v[J(J+1)]^2 + \cdots . \quad (7)$$

We determined the theoretical B_v and D_v values by calculating the vibrational levels $E_{v,J}$ for J values up to J=10 and subsequent LMSQ fitting. The first two terms of Eq. (7) gave an excellent representation of $F_v(J)$.

B. Vibration spectrum

The solution of the nuclear Schrödinger equation in Eq. (3) for J=0 yields the pure vibrational energy levels. The PEC V(R) given by Eq. (2) with the numerical parameters in column 5 of Table VII represents the total potential for the ground state of the O_2 molecule. The solution of Eq. (3) yields vibrational energy levels $G_v=E_{v,0}$ with v varying from 0 to 41. These levels G_v are reported in column two of Table VIII. Since the experimental spectroscopic data are represented in terms of the vibrational term values as $G(v)=G_v-G_0$, the latter are reported in column 3 of Table VIII. Finally, in column 4 of Table VIII, we also list the vibrational energy spacings $G_{v+1}-G_v$. Figure S3 in the supplementary material[73] displays graphically the PEC and the vibrational wave functions for v=0, v=16, and v=35.

As noted in the Introduction, the existing experimental spectroscopic data[18] for the vibrational and rotational levels

in the ground electronic state come almost entirely from observations on the very strong ($X\ ^3\Sigma_g^- - B\ ^3\Sigma_u^-$) Schumann–Runge system. The experimental spectrum has been measured in a series of papers. In 1972 Krupenie[17] published the data on the rovibrational spectrum up to v=22. More recently, the rovibrational levels from v=0 to v=28 were determined by Creek and Nicholls,[24] from v=26 to v=31 by Jongma *et al.*,[27] and from v=29 to v=35 by Yang and Wodtke.[26]

The experimental G(v) values are listed in the second column of Table IX. In this column the data for v=0–25 are taken from Ref. 24, for v=26–31 from Ref. 27, and for v =32–35 from Ref. 26. In the subsequent columns of Table IX, we list the spectra that we obtained from the following *ab initio* potentials:

- Third column, labeled "CBS:" Nonrelativistic; correlation only between the valence electrons; CBS limit.
- Fourth column, labeled "CBS+SR:" CBS from the third column plus scalar relativistic contributions.
- Fifth column labeled "CBS+SR+SO:" CBS+SR from the fourth column plus SO coupling.
- Sixth column, labeled "CBS+SR+SO+CV:" CBS +SR+SO from the fifth column plus the core-core and core-valence correlations contributions, which is in fact the full potential.

Listed in these columns (3–6) are actually the *deviations* of the theoretical from the experimental values, i.e.,

$$\Delta(v) = G(v;\text{theory}) - G(v;\text{experiment}). \tag{8}$$

The row below v=35 lists the mean absolute deviation (MAD) for each column. The last three rows in Table IX list the absolute values of the following spectroscopic quantities: the zero-point energy (ZPE), the dissociation energy D_e with respect to the lowest point on the PEC, and the equilibrium bond distance R_e corresponding to the lowest point on the PEC.

The values of the MADs in columns 3–6 of Table IX indicate that the omission of the "small corrections to the nonrelativistic valence-only-correlated complete-basis-set limit" deteriorates the MAD of the spectrum by about 70 cm^{-1}. Inclusion of the corrections is therefore essential, which is consistent with our earlier observation for the F_2 molecule.[36] The data in the sixth column indicate that the largest overall improvement is due to the core-generated correlations (about 100 cm^{-1}). For the low values v=0 to v =10, the inclusion of these correlations slightly deteriorates however the agreement with experiment, which implies some shortcomings in the treatment of the core correlations. The experimental value of D_e in Table IX is taken from Ref. 28 and the theoretical value is calculated to be within 25 cm^{-1}. It is also apparent that the inclusion of the core correlations is essential for obtaining good agreement with the experimental[95] equilibrium bond distance.

The MAD of only 12.84 cm^{-1} in the sixth column for values v=0 to v=35 reflects the high quality of the total theoretical curve. The theoretical results of Table VIII moreover predict the existence of vibrational levels up to v=41, i.e., six more levels than the experimental data available to date. Yang and Wodtke,[26] who measured the highest vibrational level v=35, estimated the levels from v=36 to v=38 using an assumed potential for V(R) and a RKR-type analysis. In view of the excellent agreement of the present theoretical spectrum with the higher experimental levels, the values for v=36 to v=41 listed in Table VIII can be expected to be more accurate than the estimates of Ref. 26. The comparison is illustrated in Fig. 6.

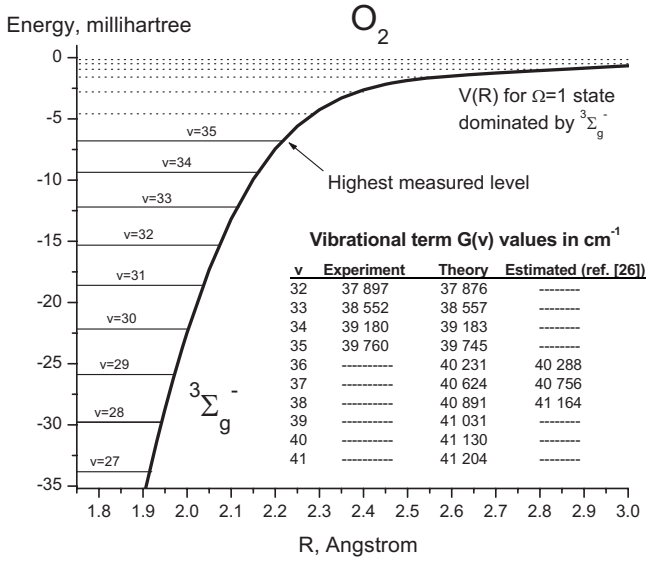

FIG. 6. Prediction of the six highest vibrational levels for the $^3\Sigma_g^-$ ground electronic state of O_2.

It should be kept in mind that the calculated vibrational spectrum is based on the spin-coupled Ω=1 component of the $^3\Sigma_g^-$ state. The transitions to the spin-coupled Ω=0 component of the $^3\Sigma_g^-$ state will exhibit small perturbations in the neighborhood of the avoided crossing with the $^1\Sigma_g^+$ state.

C. Spectroscopic rotational constants

For each vibrational quantum number v, there are many rotational levels labeled by J. We calculated the levels from J=0 to J=10 for each vibrational level v. An examination of the differences $F_v(J)=E_{vJ}-E_{vo}$ for each v as functions of $[J(J+1)]$ showed that they had the dependence expressed by Eq. (7) for J varying from 0 to 10. The coefficients B_v and D_v were determined by linear regression over this range using the expression

$$[F_v(J)/J(J+1)] = B_v - D_v[J(J+1)], \tag{9}$$

which yielded excellent fits. The results of the LMSQ fittings are reported in Table X. The experimental data for B_v (column three) and D_v (column six) are taken from Ref. 24 for v=0 to v=28, and from Ref. 27 for v=29 to v=31. The deviations of the theoretical results from the experimental data are listed in column 4 (for B_v values) and in column 7 (for D_v values). Table X reveals excellent agreement between theory and experiment for the rotational constants.

TABLE X. Theoretical and experimental rotational constants of the ground state of O_2. Energies for B_v are in cm^{-1}. Energies for D_v are in 10^{-6} cm^{-1}.

	B_v			D_v		
v	Theory[a]	Experiment[b]	δ [c]	Theory[a]	Experiment[b]	δ [c]
0	1.436 57	1.437 71	−0.001 14	5.786	4.854	0.932
1	1.420 63	1.421 96	−0.001 33	5.808	4.957	0.851
2	1.404 70	1.406 30	−0.001 60	5.826	5.000	0.826
3	1.388 79	1.390 70	−0.001 91	5.841	5.000	0.841
4	1.372 92	1.375 50	−0.002 58	5.853	5.049	0.804
5	1.357 10	1.360 40	−0.003 30	5.863	5.145	0.718
6	1.341 34	1.344 30	−0.002 96	5.870	5.006	0.864
7	1.325 63	1.328 57	−0.002 94	5.876	4.953	0.923
8	1.309 99	1.313 11	−0.003 12	5.882	4.990	0.892
9	1.294 40	1.297 76	−0.003 36	5.888	5.012	0.876
10	1.278 85	1.282 21	−0.003 36	5.896	4.990	0.906
11	1.263 34	1.266 10	−0.002 76	5.907	4.951	0.956
12	1.247 84	1.250 45	−0.002 61	5.922	4.961	0.961
13	1.232 33	1.235 26	−0.002 93	5.943	5.028	0.915
14	1.216 79	1.219 92	−0.003 13	5.971	5.100	0.871
15	1.201 17	1.204 10	−0.002 93	6.007	5.134	0.873
16	1.185 45	1.188 33	−0.002 88	6.054	5.197	0.857
17	1.169 59	1.172 65	−0.003 06	6.113	5.290	0.823
18	1.153 55	1.156 44	−0.002 89	6.186	5.356	0.830
19	1.137 26	1.140 12	−0.002 86	6.276	5.454	0.822
20	1.120 68	1.123 54	−0.002 86	6.384	5.557	0.827
21	1.103 75	1.106 81	−0.003 06	6.516	5.711	0.805
22	1.086 39	1.089 58	−0.003 19	6.673	5.880	0.793
23	1.068 51	1.072 02	−0.003 51	6.863	6.094	0.769
24	1.050 04	1.053 73	−0.003 69	7.089	6.303	0.786
25	1.030 85	1.035 02	−0.004 17	7.362	6.648	0.714
26	1.010 80	1.015 37	−0.004 57	7.691	7.024	0.667
27	0.989 75	0.994 27	−0.004 52	8.091	7.362	0.729
28	0.967 48	0.973 93	−0.006 45	8.581	8.684	−0.103
29	0.943 75	0.946 57	−0.002 82	9.190	7.100	2.090
30	0.918 23	0.920 34	−0.002 11	9.959	8.400	1.559
31	0.890 46	0.892 48	−0.002 02	10.950	9.600	1.350
32	0.859 84	⋯		12.270		⋯
33	0.825 45	⋯		14.100		⋯
34	0.785 88	⋯		16.770		⋯
35	0.738 74	⋯		21.000		⋯
36	0.679 45	⋯		28.620		⋯
37	0.597 78	⋯		45.300		⋯
38	0.474 88	⋯		77.400		⋯
39	0.377 18	⋯		43.210		⋯
40	0.334 25	⋯		47.620		⋯
41	0.272 14	⋯		98.010		⋯

[a]Theoretical B_v and D_v values are obtained from a fit of Eq. (9) to the rotational data for J=0 to J=10.
[b]See text regarding the sources.
[c]δ=(theory)−(experiment).

IV. SUMMARY

The present study of the X $^3\Sigma_g^-$ ground state of the oxygen molecule represents the second *ab initio* calculation of a rotational-vibrational spectrum for a first-row diatomic molecule with near-spectroscopic accuracy by this group. The CEEIS[96–100] method was instrumental in accomplishing this objective. The previous *ab initio* calculation of the rovibrational spectrum of the F_2 molecule[34–36] recovered the vibrational spectrum with a MAD of 5 cm^{-1}, the first *ab initio* calculation to do so.[101]

In the present series of two papers, the complete theoretical route from the *ab initio* quantum-chemical calculation of the PEC to the entire vibration-rotation spectrum has been traversed for the $^3\Sigma_g^-$ ground state of the oxygen molecule without empirical adjustments. Electron correlations involving valence electrons were calculated using the CEEIS method and the complete-basis-set limit of these nonrelativistic energies was determined. Then, electron correlations involving core electrons as well as SO coupling and scalar relativistic corrections were added. As discussed in Refs. 75,

35, and 102, respectively, spin-spin couplings and the diagonal non-Born–Oppenheimer corrections are negligible for this PEC and have therefore not been evaluated. A close analytic fit to the *ab initio* energies over the entire distance range was found by an even-tempered Gaussian expansion,[36] as had been the case of F_2, and, from it, the vibration and rotation spectrum was calculated by the DVR method.[91–93]

High-resolution electronic spectroscopy accurately established[24–27] the vibrational levels v=0 to v=35, leaving open the existence of levels with higher v values. The mean absolute mean deviation of our theoretical vibrational levels from these experimental data was found to be 12.84 cm^{-1}. In addition, we predict six more vibrational levels up to v=41. The theoretical rotational coefficients B_v and D_v were also found to agree well with the reported experimental data. The calculated dissociation energy was found to lie within 25 cm^{-1} of the experimental value reported by the most recent study of Ruscic *et al.*[28] for which an error bar of 3 cm^{-1} was quoted. Our results also predict new rotational constants for the levels v=32 to v=41.

Test calculations showed that the recovery of the experimental vibrational spectrum with a MAD of $\sim$10 cm^{-1} is contingent upon inclusion of all the contributions mentioned above: valence and core correlations, CBS extrapolation, SO coupling, and scalar relativistic contributions. Omission of any one of these will increase the mean error by orders of magnitude. This observation regarding the higher-order corrections is in agreement with our earlier work[36] and the observations of other researchers.[103–105] The intersection between the lowest $^1\Sigma_g^+$ state and the $^3\Sigma_g^-$ ground state and the attendant SO splitting, a point of some interest to spectroscopists and dynamicists, was also determined.

Experimental vibrational spectra of diatomic molecules provide very accurate information for probing energetic changes along entire reaction paths. They present therefore good tests for *ab initio* methods whose aim is the description of reaction paths. The approach followed here acquitted itself as up to the task and moreover yielded predictions regarding vibrational levels that could not yet be measured experimentally.

ACKNOWLEDGMENTS

The authors thank Dr. Michael W. Schmidt for his lively interest, his stimulating critique, and his many valuable suggestions. K.R. thanks Professor R. W. Field for a series of illuminating discussions. The present work was supported by the Division of Chemical Sciences, Office of Basic Energy Sciences, U.S. Department of Energy under Contract No. DE-AC02-07CH11358 with Iowa State University through the Ames Laboratory. The authors also acknowledge support from the Department of Energy PCTC program (PI: Mark Gordon).

[1] D. J. Des Marais, Science **289**, 1703 (2000).
[2] G. C. Dismukes, V. V. Klimov, S. V. Baranov, Yu. N. Kozlov, J. DasGupta, and A. Tyryshkin, Proc. Natl. Acad. Sci. U.S.A. **98**, 2170 (2001).
[3] A. H. Knoll, Geobiology **1**, 3 (2003).
[4] J. Raymond and D. Segrè, Science **311**, 1764 (2006).
[5] K. P. Jensen and U. Ryde, J. Biol. Chem. **279**, 14561 (2004).
[6] M. J. Paterson, O. Christiansen, F. Jensen, and P. R. Ogilby, Photochem. Photobiol. **82**, 1136 (2006).
[7] D. H. Parker, Acc. Chem. Res. **33**, 563 (2000).
[8] A. J. Alexander, Z. H. Kim, and R. N. Zare, J. Chem. Phys. **118**, 10566 (2003).
[9] R. Takegami and S. Yabushita, J. Mol. Spectrosc. **229**, 63 (2005).
[10] M. C. G. N. van Vroonhoven and G. C. Groenenboom, J. Chem. Phys. **116**, 1954 (2002).
[11] M. C. G. N. van Vroonhoven and G. C. Groenenboom, J. Chem. Phys. **117**, 5240 (2002).
[12] R. S. Mulliken, Rev. Mod. Phys. **4**, 1 (1932).
[13] R. Rydberg, Z. Phys. **73**, 376 (1931); O. Klein, *ibid.* **76**, 226 (1932); A. L. G. Rees, Proc. Phys. Soc. London **59**, 998 (1947).
[14] J. T. Vanderslice, E. A. Mason, and W. G. Maisch, J. Chem. Phys. **32**, 515 (1960).
[15] J. Tellinghuisen, Comput. Phys. Commun. **6**, 221 (1973).
[16] J. M. Merritt, V. E. Bondybey, and M. C. Heaven, Science **324**, 1548 (2009).
[17] P. H. Krupenie, J. Phys. Chem. Ref. Data **1**, 423 (1972).
[18] T. G. Slanger and P. C. Cosby, J. Phys. Chem. **92**, 267 (1988).
[19] T. G. Slanger and R. A. Copeland, Chem. Rev. (Washington, D.C.) **103**, 4731 (2003).
[20] V. Schumann, Smithsonian Contrib. Knowl. **29**, 1413 (1903).
[21] C. Runge, Physica **1**, 254 (1921).
[22] H. P. Knauss and S. S. Ballard, Phys. Rev. **48**, 796 (1935).
[23] C. E. Treanor and W. H. Wurster, J. Chem. Phys. **32**, 758 (1960).
[24] D. M. Creek and R. W. Nicholls, Proc. R. Soc. London, Ser. A **341**, 517 (1975).
[25] C. P. Chen and D. A. Ramsay, J. Mol. Spectrosc. **160**, 512 (1993).
[26] X. Yang and A. M. Wodtke, J. Chem. Phys. **90**, 7114 (1989).
[27] R. T. Jongma, S. Shi, and A. M. Wodtke, J. Chem. Phys. **111**, 2588 (1999).
[28] B. Ruscic, R. E. Pinzon, M. L. Morton, G. von Laszevski, S. J. Bittner, S. G. Nijsure, K. A. Amin, M. Minkoff, and A. F. Wagner, J. Phys. Chem. A **108**, 9979 (2004).
[29] P. Brix and G. Herzberg, Can. J. Phys. **32**, 110 (1954).
[30] C. Pernot, J. Durup, J.-B. Ozenne, J. A. Beswick, P. C. Cosby, and J. T. Moseley, J. Chem. Phys. **71**, 2387 (1979).
[31] S. T. Gibson, B. R. Lewis, K. G. Baldwin, and J. H. Carver, J. Chem. Phys. **94**, 1060 (1991).
[32] P. C. Cosby and D. L. Huestis, J. Chem. Phys. **97**, 6108 (1992).
[33] L. Bytautas, K. Ruedenberg, J. Chem. Phys. **132**, 074109 (2010).
[34] L. Bytautas, T. Nagata, M. S. Gordon, and K. Ruedenberg, J. Chem. Phys. **127**, 164317 (2007).
[35] L. Bytautas, N. Matsunaga, T. Nagata, M. S. Gordon, and K. Ruedenberg, J. Chem. Phys. **127**, 204301 (2007).
[36] L. Bytautas, N. Matsunaga, T. Nagata, M. S. Gordon, and K. Ruedenberg, J. Chem. Phys. **127**, 204313 (2007).
[37] L. Bytautas and K. Ruedenberg, J. Chem. Phys. **130**, 204101 (2009).
[38] S. L. Guberman, J. Chem. Phys. **67**, 1125 (1977).
[39] A. J. C. Varandas, Chem. Phys. Lett. **443**, 398 (2007).
[40] R. P. Saxon and B. Liu, J. Chem. Phys. **67**, 5432 (1977).
[41] H. Partridge, C. W. Bauschlicher, Jr., S. R. Langhoff, and P. R. Taylor, J. Chem. Phys. **95**, 8292 (1991).
[42] T. Müller, M. Dallos, H. Lischka, Z. Dubrovay, and P. G. Szalay, Theor. Chem. Acc. **105**, 227 (2001).
[43] B. Mintz, T. G. Williams, L. Howard, and A. K. Wilson, J. Chem. Phys. **130**, 234104 (2009).
[44] T. H. Dunning, Jr., J. Chem. Phys. **90**, 1007 (1989).
[45] K. A. Peterson, A. K. Wilson, D. E. Woon, and T. H. Dunning, Jr., Theor. Chem. Acc. **97**, 251 (1997).
[46] A. Halkier, T. Helgaker, P. Jørgensen, W. Klopper, H. Koch, J. Olsen, and A. K. Wilson, Chem. Phys. Lett. **286**, 243 (1998).
[47] W. Klopper, B. Ruscic, D. P. Tew, F. A. Bischoff, and S. Wolfsegger, Chem. Phys. **356**, 14 (2009).
[48] M. W. Schmidt, K. K. Baldridge, J. A. Boatz, S. T. Elbert, M. S. Gordon, J. H. Jensen, S. Koseki, N. Matsunaga, K. A. Nguyen, S. J. Su, T. L. Windus, M. Dupuis, and J. A. Montgomery, J. Comput. Chem. **14**, 1347 (1993).
[49] M. S. Gordon and M. W. Schmidt, in *Theory and Applications of Computational Chemistry: The First Forty Years*, edited by C. E. Dykstra, G. Frenking, K. S. Kim, and G. E. Scuseria (Elsevier, Amsterdam, 2005), p. 1167.
[50] K. Ruedenberg, M. W. Schmidt, M. M. Gilbert, and S. T. Elbert, Chem. Phys. **71**, 41 (1982).

[51] M. Douglas and N. M. Kroll, Ann. Phys. **82**, 89 (1974).
[52] B. A. Hess, Phys. Rev. A **33**, 3742 (1986).
[53] G. Jansen and B. A. Hess, Phys. Rev. A **39**, 6016 (1989).
[54] D. G. Fedorov, S. Koseki, M. W. Schmidt, and M. S. Gordon, Int. Rev. Phys. Chem. **22**, 551 (2003).
[55] R. D. Cowan and D. C. Griffin, J. Opt. Soc. Am. **66**, 1010 (1976).
[56] A. Rutkowski, J. Phys. B **19**, 149 (1986).
[57] E. Ottschofski and W. Kutzelnigg, J. Chem. Phys. **106**, 6634 (1997).
[58] T. Nakajima and K. Hirao, Monatsh. Chem. **136**, 965 (2005).
[59] T. Nakajima and K. Hirao, Chem. Phys. Lett. **302**, 383 (1999).
[60] T. Nakajima, K. Koga, and K. Hirao, J. Chem. Phys. **112**, 10142 (2000).
[61] D. G. Fedorov, T. Nakajima, and K. Hirao, Chem. Phys. Lett. **335**, 183 (2001).
[62] D. G. Fedorov and M. S. Gordon, J. Chem. Phys. **112**, 5611 (2000).
[63] C. M. Marian, Rev. Comput. Chem. **17**, 99 (2001).
[64] T. Helgaker, W. Klopper, and D. P. Tew, Mol. Phys. **106**, 2107 (2008).
[65] T. R. Furlani and H. F. King, J. Chem. Phys. **82**, 5577 (1985).
[66] A. Nicklass, K. A. Peterson, A. Berning, H.-J. Werner, and P. J. Knowles, J. Chem. Phys. **112**, 5624 (2000).
[67] R. Klotz and S. D. Peyerimhoff, Mol. Phys. **57**, 573 (1986).
[68] B. F. Minaev, Phys. Chem. Chem. Phys. **1**, 3403 (1999).
[69] B. F. Minaev and L. B. Yashchuk, Opt. Spectrosc. **95**, 553 (2003).
[70] E. Wigner and E. E. Witmer, Z. Phys. **51**, 859 (1928).
[71] F. Hund, Z. Phys. **63**, 723 (1930).
[72] F. R. Gilmore, "Potential energy curves for N_2, NO, O_2, and corresponding ions," RAND Corporation Memorandum No. R-4034-PR, 1964.
[73] See supplementary material at http://dx.doi.org/10.1063/1.3298376 for additional tables and figures.
[74] C. E. Moore, *Atomic Energy Levels* (National Bureau of Standards, Washington D.C., 1971).
[75] O. Vahtras, O. Loboda, B. Minaev, H. Ågren, and K. Ruud, Chem. Phys. **279**, 133 (2002).
[76] R. L. Miller, A. G. Suits, P. L. Houston, R. Toumi, J. A. Mack, and A. M. Wodtke, Science **265**, 1831 (1994).
[77] P. J. Crutzen, J. U. Grooß, C. Brühl, R. Müller, and J. M. Russell III, Science **268**, 705 (1995).
[78] M. E. Summers, R. R. Conway, D. E. Siskind, M. H. Stevens, D. Offermann, M. Riese, P. Preusse, D. F. Strobel, and J. M. Russell III, Science **277**, 1967 (1997).
[79] F. Dayou, M. I. Hernández, J. Campos-Martínez, and R. Hernández-Lamoneda, J. Chem. Phys. **126**, 194309 (2007).
[80] H. Nakano, J. Chem. Phys. **99**, 7983 (1993).
[81] H. Nakano, Chem. Phys. Lett. **207**, 372 (1993).
[82] R. Hernández-Lamoneda and A. Ramírez-Solís, Chem. Phys. Lett. **321**, 191 (2000).
[83] H. Lefebvre-Brion and R. W. Field, *Perturbations in the Spectra of Diatomic Molecules* (Academic, New York, 1986).
[84] J. F. Ogilvie, *The Vibrational and Rotational Spectrometry of Diatomic Molecules* (Academic, New York, 1998).
[85] H. Müller, R. Franke, S. Vogtner, R. Jaquet, and W. Kutzelnigg, Theor. Chem. Acc. **100**, 85 (1998).
[86] R. D. Bardo and K. Ruedenberg, J. Chem. Phys. **59**, 5956 (1973).
[87] D. F. Feller and K. Ruedenberg, Theor. Chim. Acta **52**, 231 (1979).
[88] M. W. Schmidt and K. Ruedenberg, J. Chem. Phys. **71**, 3951 (1979).
[89] See, e.g., L. Pauling and E. B. Wilson, *Introduction to Quantum Mechanics* (McGraw-Hill, New York, 1935).
[90] National Institute of Standards and Technology, Physics Laboratory, Physical Reference Data, Atomic Weights and Isotopic Compositions, 2005; http://physics.nist.gov/PhysRefData/Compositions/.
[91] J. C. Light, I. P. Hamilton, and J. V. Lill, J. Chem. Phys. **82**, 1400 (1985).
[92] Z. Bačić and J. C. Light, J. Chem. Phys. **85**, 4594 (1986).
[93] D. T. Colbert and W. H. Miller, J. Chem. Phys. **96**, 1982 (1992).
[94] B. S. Garbow, J. M. Boyle, J. J. Dongarra, and C. B. Moler, *EISPACK Guide Extension Lecture Notes in Computer Science* (Springer, New York, Heidelberg, Berlin, 1977), Vol. 51; http://www.netlib.org/eispack/
[95] K. P. Huber and G. Herzberg, *Molecular Spectra and Molecular Structure. IV. Constants of Diatomic Molecules* (Van Nostrand Reinhold, New York, 1979).
[96] L. Bytautas and K. Ruedenberg, J. Chem. Phys. **121**, 10905 (2004).
[97] L. Bytautas and K. Ruedenberg, J. Chem. Phys. **121**, 10919 (2004).
[98] L. Bytautas and K. Ruedenberg, J. Chem. Phys. **121**, 10852 (2004).
[99] L. Bytautas and K. Ruedenberg, J. Chem. Phys. **122**, 154110 (2005).
[100] L. Bytautas and K. Ruedenberg, J. Chem. Phys. **124**, 174304 (2006).
[101] M. W. Justik, Annu. Rep. Prog. Chem., Sect. A: Inorg. Chem. **104**, 134 (2008).
[102] J. Gauss, A. Tajti, M. Kállay, J. F. Stanton, and P. G. Szalay, J. Chem. Phys. **125**, 144111 (2006).
[103] G. Tarczay, A. G. Császár, W. Klopper, and H. M. Quiney, Mol. Phys. **99**, 1769 (2001).
[104] O. L. Polyansky, A. G. Császár, S. V. Shirin, N. F. Zobov, P. Barletta, J. Tennyson, D. W. Schwenke, and P. J. Knowles, Science **299**, 539 (2003).
[105] S. Hirata, T. Yanai, R. J. Harrison, M. Kamiya, and P.-D. Fan, J. Chem. Phys. **126**, 024104 (2007).